metals

MDPI

Article

Fracture Toughness Analysis of Automotive-Grade Dual-Phase Steel Using Essential Work of Fracture (EWF) Method

Sunil Kumar M R [1,*], Eva Schmidova [1], Pavel Konopík [2], Daniel Melzer [2], Fatih Bozkurt [3] and Neelakantha V Londe [4]

1 Faculty of Transport Engineering, University of Pardubice, 53210 Pardubice, Czech Republic; Eva.schmidova@upce.cz
2 Mechanical Testing and Thermophysical Measurement, COMTES FHT a.s., 33441 Dobřany, Czech Republic; pavel.konopik@comtesfht.cz (P.K.); daniel.melzer@comtesfht.cz (D.M.)
3 Vocational School of Transportation, Eskisehir Technical University, 26140 Eskisehir, Turkey; fatihbozkurt@eskisehir.edu.tr
4 Department of Mechanical Engineering, Mangalore Institute of Technology & Engineering, Moodabidre 574225, India; nvlondhe@gmail.com
* Correspondence: sunilmr21@gmail.com; Tel.: +420-777-95-5826

Received: 2 July 2020; Accepted: 27 July 2020; Published: 29 July 2020

Abstract: Fracture toughness determination of dual-phase DP450 steel using the essential work of fracture (EWF) methodology is the major focus of this research work. The EWF method is used for the determination of fracture toughness of thin sheets in a plane stress dominant condition. The EWF method is discussed in detail with the help of DP450 steel experimental results. Double edge notched tension (DENT) specimens with fatigue pre-crack and without fatigue crack (notched) have been used for testing. Specific essential work of fracture (w_e), crack tip opening displacement (δ_c^e) and crack tip opening angle (ψ^e) parameters were used for the comparative analysis. High-intensity laser beam cutting technology was used for the preparation of notches. Fracture toughness values of fatigue pre-cracked and notched samples were compared. The effect of notch tip radius and fatigue crack on the fracture toughness values were analysed. Digital image correlation (DIC) technology was used for the identification of local strain distribution and validation of the methodology. Fractured surfaces were examined by a scanning electron microscope (SEM) to analyse the fracture morphology and stress state.

Keywords: essential work of fracture (EWF); double edge notch tension (DENT); DP450; fracture toughness

1. Introduction

The automotive industry is under constant pressure to increase the efficiency of vehicles, reduce emissions and get better crashworthiness. Various public norms, as well as competition, are the driving forces. Weight reduction is achieved by using new generation advanced high strength steels (AHSS) [1]. These steels have high strength compared to conventional steels. Steels used for the manufacturing of white-in-body doors and hood are required to have high strength, as well as better formability, weldability, corrosion resistance and fracture toughness. Dual-phase (DP) steel is one of the new generation steels with a high ultimate strength to yield strength ratio. Dual-phase steel primarily contains ferrite structure and islands of martensite, achieved through heat treatment and the addition of alloying elements. Martensite content increases the strength of the steel, meanwhile, the ferrite

content gives ductility to the steel [2,3]. Dual-phase steel is better suitable for stamping applications due to its high ultimate strength to yield strength ratio [4,5].

During the stamping of automotive components, materials with low fracture toughness often develop new edge cracks or pre-existing minute cracks, formed during shear cutting, piercing and trimming of sheets, which may grow. Material fracture toughness of has a direct influence on edge cracking resistance [6] and crashworthiness in passive safety. The forming limit diagram (FLD) is an excellent choice to identify necking during stamping applications. However, FLD does not emphasise fracture toughness or edge cracking resistance. The determination of fracture toughness is vital for material selection in stamping applications.

The international ASTM E399 [7] (linear elastic plane strain fracture toughness) standard uses plane strain dominant condition to keep plastic deformation low and constant. The fracture toughness value obtained from this method is independent of thickness. Due to its minimum thickness restriction ($1 \leq W/B \leq 4$ range for various specimens) and plastic size restriction, this standard is not feasible for thin samples. The ASTM E1820 [8] standard measurement of fracture toughness (J-integral and CTOD) is ideal for elastic–plastic material. The minimum thickness constraint is less restrictive than E399; although, automotive thin steel sheets do not fulfil the thickness requirement. ASTM E561 [9] (K–R curve) could be used for thin sheets, as it does not have any thickness restriction. However, the results are thickness sensitive. The results from the above standard have no single critical value, unlike K_{Ic} or J_c. Fracture resistance is dependent on the stress field in front of the crack tip. Thicker sections of the same material may exhibit less resistance to the crack growth, one of the main reasons of which is the plane strain dominant condition [10]. To find out the fracture toughness of thin sheets in their original sheet thickness, the essential work of fracture (EWF) method is used. Double edge notch tension (DENT) specimens are used in the experiments.

Broberg first explained the concept of different energy zones near the crack tip [11]. Broberg divided the crack tip into two regions, namely the fracture process zone (FPZ) and outer plastic zone. Energy consumed in the FPZ is spent to create two new surfaces. FPZ is independent of crack tip stresses or loading condition. The outer plastic zone depends on the stress state, crack length, loading and geometry. The essential work of the fracture concept was first proposed by Cotterell and Reddel in 1976 [12]. Cotterell and Reddel used the Broberg concept of energy consumed in the independent autonomous end region (FPZ) as material property for the sheet thickness. In Linear elastic fracture mechanics, the plastic region around the crack tip is assumed to be very small. In ductile materials, the plastic region is large and dependent on various loading parameters. The autonomous end region in ductile materials can be characterised by necking.

Marchal and Delannay performed EWF experiments on zinc sheets under varying conditions like deformation rate, thickness, grain size and rolling direction [13]. Marchal and Delannay observed better linearity in specific essential work of fracture for different ligament lengths but expressed their concern on the hypothesis of EWF about zone separation (FPZ and outer plastic zone). Chandra et al. [14] have worked on the essential work of fracture method for interstitial free steel and determined specific essential work of fracture, crack tip opening displacement (CTOD) and crack tip opening angle (CTOA). The ESIS protocols [15,16] conducted in round-robin experiments on polymers give enhancing knowledge about dimensions and parameters affecting the EWF results. Golling et al. [17] have conducted experiments using the EWF method at a higher loading rates on different AHSS and found the specific essential work of fracture increases with an increase in the loading rate. Frómeta et al. [18] conducted experiments to relate the essential work of fracture and crash resistance of automotive steels. Materials with higher fracture toughness values obtained from the EWF test showed better crash resistance. Several researchers simulated the EWF test in FEM analysis to find the influence of various parameters on fracture toughness [19–21]. Some researchers have even attempted to compare the specific essential work of fracture w_e with critical J_c integral [22]. Rink et al. [23] calculated and compared J_c and w_e for different polymers using the Begley–Landes method and EWF method,

respectively. w_e is obtained from fracturing the entire ligament and represents both initiation and crack propagation resistance. While the J_c value is highly dependent on a small crack extension resistance.

In the EWF method, energy absorbed by the specimen to completely fracture it is the work of fracture. The area under the load–displacement curve is equivalent to work of fracture (W_f). The total work of fracture is divided into two energies (Equation (1)), essential energy and non-essential energy, respectively.

$$W_f = W_e + W_p \tag{1}$$

Essential work of fracture (W_e) is the energy consumed by the fracture process zone; it is a factor of the area along the crack path. The non-essential work of fracture (W_p) is the energy consumed by the plastic deformation; it is a function of the volume of the plastic zone.

$$W_f = w_e L t + w_p L^2 t \beta \tag{2}$$

In Equation (2), w_e is the specific essential work of fracture, w_p is the specific non-essential work of fracture, L is the ligament length, t is the thickness of the sheet and β is the plastic zone shape factor, which is $\frac{\pi}{4}$ for the circular shape. If the whole Equation (2) is divided by the area of the ligament, then,

$$w_f = \frac{W_f}{Lt} = w_e + w_p L \beta \tag{3}$$

In Equation (3), w_f is the specific work of fracture energy; it is a linear function of the ligament length with slope $w_p \beta$. The value of w_e can be calculated by testing samples of different ligament lengths. In the plot of w_f versus ligament length, the value of w_e is the ordinate at zero ligament length. Theoretical background and related experiments regarding EWF methodology can be found in the literature [24–27]. The energy spent in FPZ, w_e, can further be divided into final separation energy and necking energy, but it is beyond the scope of this paper.

The primary focus of the EWF test is to find the specific essential work of fracture (w_e). Cotterell proposed parameters, such as crack tip opening displacement (δ_c^e or CTOD) and crack tip opening angle (ψ^e or CTOA), based on the elongation data during EWF test [27]. The CTOD and CTOA obtained from the EWF test, compared to the standard test, have little constraints and are purely dependent on FPZ. The total elongation of the sample in terms of CTOD and CTOA is written in Equation (4).

$$u_f = \delta_c^e + \frac{\psi^e}{2} L \tag{4}$$

In the plot of total elongation versus ligament length, the ordinate at zero ligament length is equal to the crack tip opening displacement (δ_c^e or CTOD). The slope of the curve is equal to the half-subtended angle by two surfaces ($\frac{\psi^e}{2}$) in FPZ.

Faccoli et al. [28] and Kamat et al. [29] conducted experiments to relate the critical *J*-integral J_c with notch tip radius ρ. The value of critical J_c integral increases with an increase in notch tip radius. The value of J_c integral will become insensitive to the notch tip radius below the critical value ρ_c. The determination of ρ_c is quite challenging and depends on various factors. There is no established standard to relate notch tip radius and fracture toughness. To determine the effect of notch tip radius on specific essential work of fracture, a notch tip radius of 55 µm was selected and the results are compared with fatigue cracked samples. Generally, ASTM standards suggest EDM technology for notch preparation. In this work, high intensity laser technology is used for notch preparations to ensure the lowest possible radius without significantly affecting the material properties.

To verify the state of plane stress during the loading, the maximum stress in the ligament should be independent of ligament length. This criterion can be analysed using Hill's theory [30] of ideal elastic–plastic materials. The maximum stress along the ligament should be in the range of $1.15\sigma_Y > \sigma > 0.9\sigma_Y$ [15]. Due to excessive strain hardening, the stresses are far higher. The yield

strength cannot be used as a limiting criterion here. The yield strength is replaced by the ultimate strength to verify the plane stress state in the ligament length [14].

2. Material and Experimental Details

2.1. Material

The dual-phase DP450 steel used in this research work comprises a maximum chemical composition in percent by weight, exclusive of iron, of 0.083% carbon, 1.72% manganese, 0.026% silicon, 0.209% chromium, 0.163% titanium, 0.056% aluminium, 0.021% phosphorus and 0.014% copper. The microstructure of DP450 is shown in Figure 1. DP450 steel has yield strength (σ_y) of 290 MPa, ultimate strength (σ_u) of 480.60 MPa, elongation at fracture (A_{50}%) of 30.36%, elongation at ultimate stress (A_g%) of 18.81% and strain hardening exponent (n) of 0.18. The standard engineering stress–strain curve for DP450 steel is shown in Figure 2. The large dark grains in Figure 1 are ferrite and shiny small islands of martensite are located close to the grain boundaries. The strength of DP450 steel is on the lower band compared to other dual-phase steels. The martensitic volume fraction is relatively low compared to other dual-phase steels [2]. Low carbon content in the material is attributed to the presence of large ferrite volume fraction. The 1.72% manganese count helps in stabilising the premature formation of martensite and strengthens the ferrite [31].

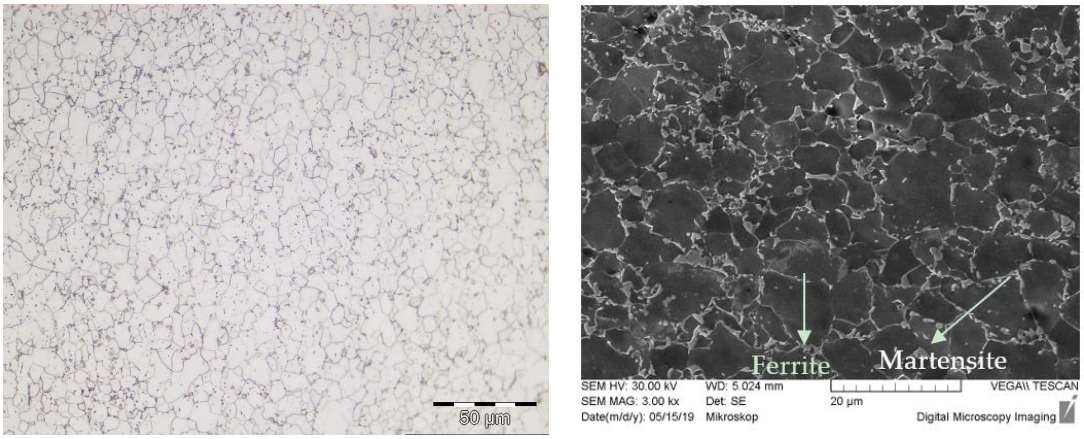

(**a**) (**b**)

Figure 1. Microstructure of DP450 steel: (**a**) Optical microscope image; (**b**) Scanning electron microscope image.

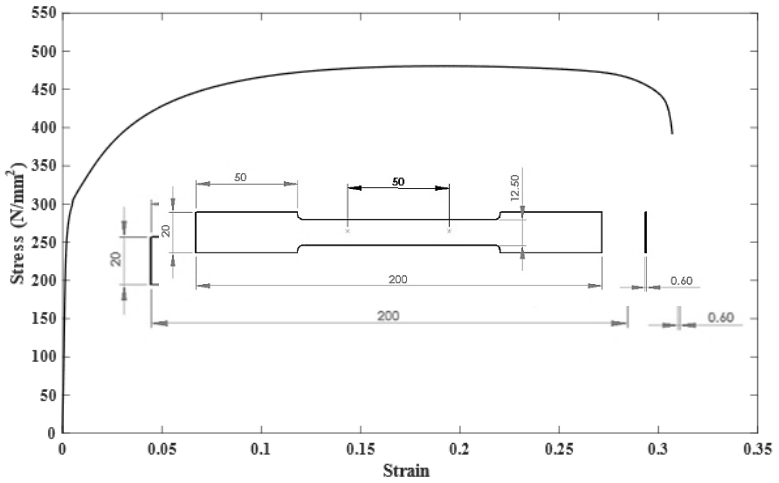

Figure 2. Engineering stress–strain curve of DP450 steel with specimen scheme (mm).

2.2. Specimen

The double-edge notched tension (DENT) specimen was chosen for the experiments. Transverse stress in the ligament between notches is tensile; hence, no anti-buckling plates were required. Figure 3a shows the simple schematic representation of the DENT specimen used in the experiments. The specimen has a general dimension of 45 mm width, 150 mm height and 0.6 mm thickness with a 30 mm gripping section on either side. Ligament lengths were chosen in the range between $5t < L < W/3$ (t is the thickness of the specimen; W is the width of the specimen). The lower limit of the ligament length is to avoid the quasi-plain strain condition, and the higher limit of the ligament is to avoid the formation of two separate plastic zones [12]. Nine samples were prepared to have a ligament length from five to thirteen millimetres. Specimens were prepared using high-intensity laser cutting. The notch tip radius is 55 µm and it is shown in Figure 3b. Fatigue cracks are created in the samples using cycling loading in a fatigue machine. The ASTM E399 [7] recommends that the maximum stress intensity factor during fatigue pre-crack shall not exceed 80% for crack initiation and 60% for the terminal stage of the critical stress intensity factor. Since K_{Ic} is not an appropriate limit for thin ductile sheet material, a more conservative parameter yield stress was used as a critical parameter. The maximum stress in the ligament was kept below 80% of the yield stress. Thereby, the maximum load during fatigue crack initiation was kept well below the critical stress intensity factor to avoid low cycle fatigue. The direction of loading was changed for every few thousand cycles to get equal crack growth on either side of the notch. The length of the fatigue crack was about 1 mm on either side.

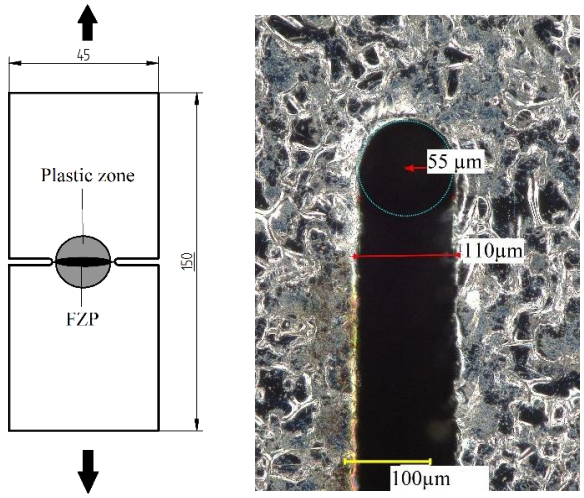

Figure 3. Double edge notched tension (DENT) specimen: (**a**) Schematic representation of the specimen (mm); (**b**) Notch tip geometries of the specimen (digital microscope).

2.3. EWF Testing

The standard mechanical properties of the material were determined by testing three dog bone-shaped samples according to ASTM E8/E8M [32] and average values were taken (Section 2.1). The standard strain rate of 0.002 s^{-1} and a gauge length of 50 mm were used. An in-built extensometer measured accurate displacement during tensile testing.

To determine the specific essential work of the fracture using DENT specimens, the specimen was pulled in Zwick Z030 universal tensile testing machine (ZwickRoell GmbH, Ulm, Germany) until the final fracture. The displacement of the specimen during EWF testing was automatically recorded by the crosshead movement. The crosshead speed of 1 mm/min was used as the standard in all tests. The grip on either end was limited to a maximum of 30 mm. To analyse the strain distribution in the ligament and validate the EWF methodology, ARAMIS digital image correlation technology (DIC)

(GOM GmbH, Braunschweig, Germany) was used. A stochastic pattern was created on the specimens using white and black synthetic spray paints. A series of images were taken (up to 10 images per second) with the help of two cameras in the DIC system. These images were then automatically computed and post-processed by the ARAMIS software (version 6.3, GOM GmbH, Braunschweig, Germany). The local strain distribution, displacements and necking of the specimen were evaluated using the DIC system [33].

3. Results and Discussions

3.1. Essential Work of Fracture

Figure 4 shows the force versus displacement curve for all ligament lengths ranging from 5 mm to 13 mm. All curves follow an identical curve shape. In addition, from the graph it clear that large plastic deformation happened before and after reaching the maximum force. The maximum stress in the ligament is plotted against ligament length for various samples and is shown in Figure 5. The variation of stress for all ligament lengths is in the earlier-specified range (introduction), which is an empirical indication of similar stress states in all samples.

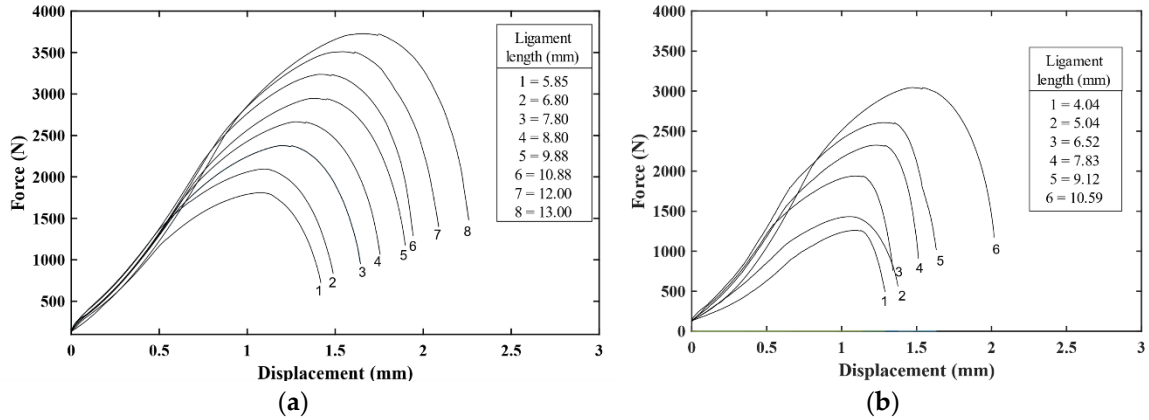

Figure 4. Force–displacement graph for all ligament lengths for: (**a**) Notched specimens; (**b**) Fatigue pre-cracked specimens.

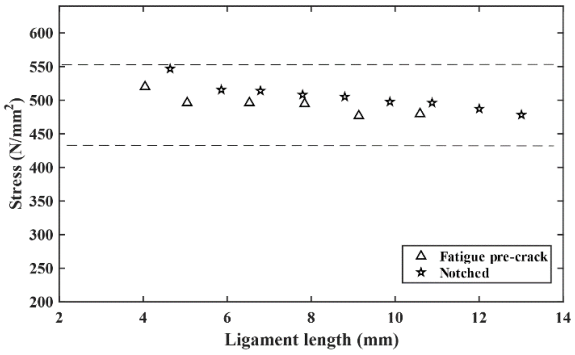

Figure 5. Maximum stress versus ligament length for all DENT specimens.

The area under the force–displacement diagram is the work of fracture W_f. The work of fracture is calculated by the direct integration of the curve data. The values of specific essential work of fracture w_f is plotted against the ligament length to find the essential work of fracture w_e (Figure 6). The detailed results are tabulated in Table 1. The value of w_e is 230.45 kJ/m^2 for fatigue pre-cracked samples. The value of w_e is 332.3 kJ/m^2 for notched samples. The introduction of fatigue crack into the sample reduced the specific essential work of fracture by about 30%. The specific essential work of fracture results are highly dependent on the presence of fatigue crack, and a w_e value calculated

without fatigue crack would overestimate the results. The value of w_e is dependent on the thickness of the specimen and generally increases linearly with thickness [34]. The value of w_f for a shorter ligament length is slightly offset of the regression line because of the increased ratio of transitional distance to uniform necking length. The chosen lower ligament length will have a considerable effect on w_e result. The experimental results show that the fracture toughness values are still sensitive to the notch tip radius. The critical notch tip radius ρ_c is much lower than 55 µm. The R-values indicate good linearity of the results for all kinds of samples and notched samples showed better linearity. The value of $w_p\beta$ is higher for fatigue pre-cracked samples compared to notched samples.

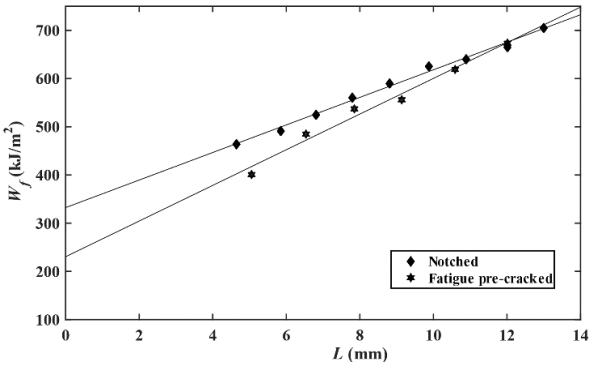

Figure 6. Specific work of fracture versus ligament length for notched and fatigue pre-cracked specimens.

Table 1. Essential work of fracture experimental results.

Type	$w_s = w_e + w_pL\beta$			$u_f = \delta_c^e + \frac{\psi^e}{2}L$		
	w_e (kJ/m^2)	$w_p\beta$ (kJ/m^3)	R	δ_c^e(mm)	$\psi^e/2$ (ψ^ein θ°)	R
Fatigue pre-cracked	230.45	36.99	0.9836	0.4088	0.1517 (17.38°)	0.9883
Notched	332.3	28.59	0.9966	0.6891	0.1192 (13.65°)	0.9956

Extrapolating the plot of displacement at the final fracture versus ligament length gives CTOD and CTOA (Figure 7). CTOD for the fatigue pre-cracked specimen is 0.4088 mm, and the same for the notched sample is 0.6891 mm. The presence of fatigue cracks in the samples decreased the CTOD by about 40%. However, in the case of CTOA, the difference between the fatigue pre-cracked and notched sample is not significant.

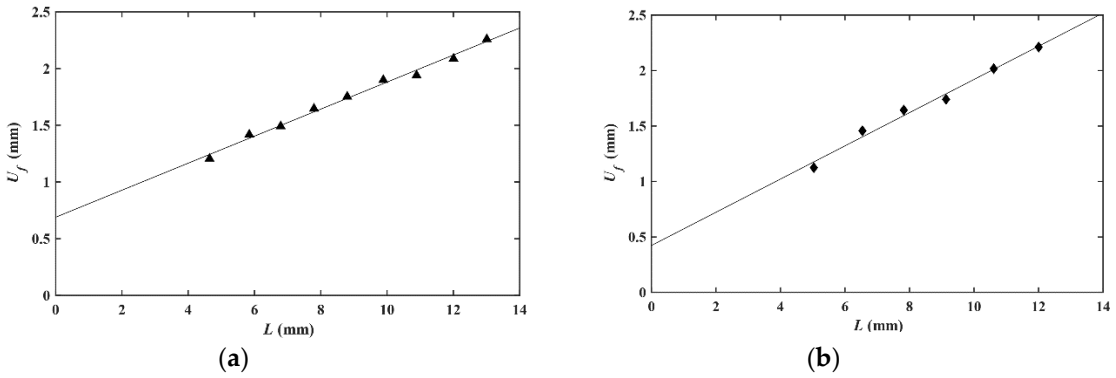

Figure 7. Elongation at fracture versus ligament length for: (**a**) notched specimens; (**b**) fatigue pre-cracked specimens.

3.2. Fractured Surfaces

Scanning electron microscope images of fractured surfaces reveal the fracture morphology during the crack propagation. Figure 8 shows the ductile fracture morphology of tested specimens, which means that micro voids nucleation and coalescence happened ahead of crack opening. Necking is minimal at the beginning of crack growth and gradually increases over a short distance (transitional distance) to a uniform level. The crack begins in quasi-plane strain condition and shifts to plane stress after the transitional distance [35]. The transitional distance is the same for all the ligament lengths and increases with thickness [27]. The presence of a fatigue crack does not significantly change the stress state at the crack tip or transitional distance. A small flat ductile fracture is observed in the middle of the fractured surface and a shear lipped slant fracture at the edges. The slant fracture proportion increases along the crack path and becomes uniform after some distance. The relative proportion of flat and slant fracture depends on strain hardening before crack initiation, fracture strain and stress state at the crack tip. The fractured surfaces show that the concept of pure plane stress does not exist in the ligament, plane stress and plane strain only exist in relative proportions to thickness. Dimples in the middle flat fracture are circular and in mode-I fracture. At the edge, dimples are mostly parabolic and in shear mode fracture. Dimples at the extreme edges almost disappeared.

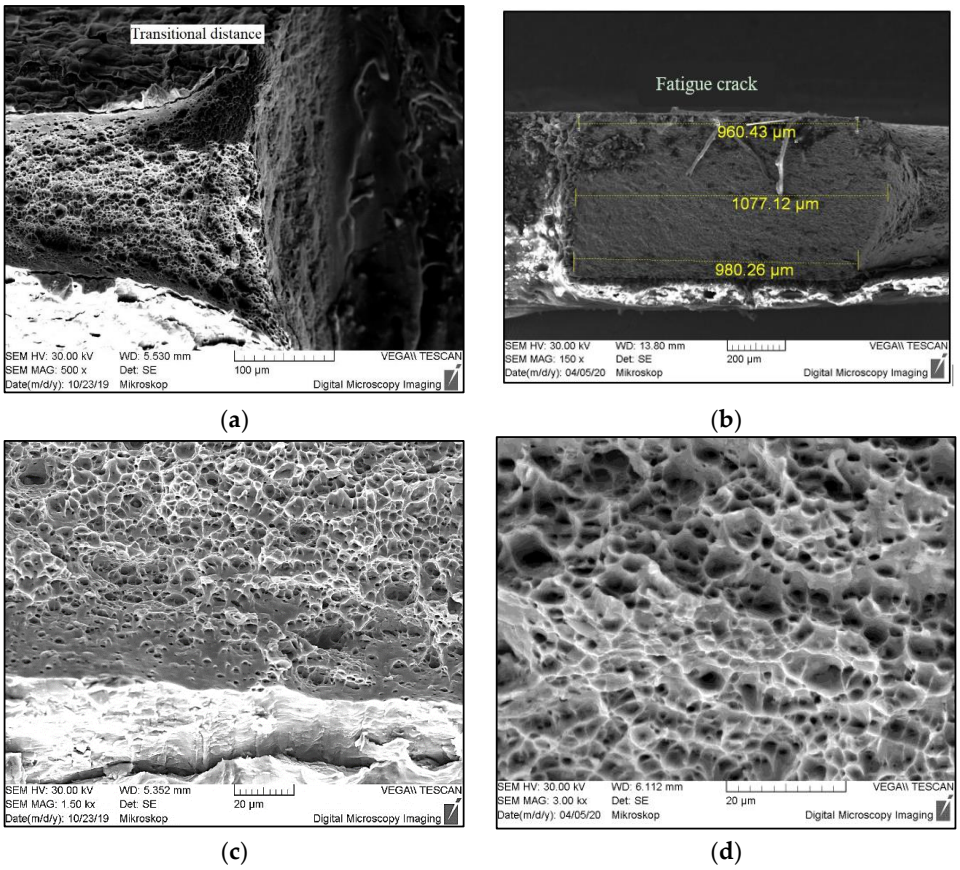

Figure 8. Scanning electron microscope (SEM) images of the fractured surface after essential work of fracture (EWF) testing: (**a**) Crack tip of a notched sample; (**b**) Crack tip of a fatigue pre-cracked sample; (**c**) Ductile and slant fracture at edge; (**d**) Flat and ductile fracture at centre.

3.3. Digital Image Correlation Results

The distribution of strain during EWF testing is evaluated using the digital image correlation technique. One of the fundamental requirements of the EWF test is limiting the plastic deformation to only the ligament and crack initiation after complete yielding of the ligament; it is verified successfully on every single test using DIC systems. Aside from around the ligament length, the rest of the specimen

has close to zero strain. Generally, crack initiation happens near peak load (notched samples) and loading in the ligament decreases as the crack propagates. For fatigue pre-cracked samples, the crack initiated before reaching the peak load. Generally, in all tests, the crack propagated at the same speed in either direction. The highest strain concentration can be found at notches and advances as the crack propagates (Figure 9). The shape of the plastic deformation around the ligament is circular for lower length ligaments and becomes more elliptical for longer ligament lengths. Figure 10 shows the Von-Mises strain just before crack initiation for various ligament lengths (scaling factor is set between zero and log 0.1). The maximum strain is only concentrated in the fracture process zone and the strain is distributed in incremental bands connecting two notches. In Figure 11, the major strain along a section line is plotted at a different time interval. The peak strain at the middle of the sectional line is the indication of extensive necking before fracture in FPZ. The major strain distribution is mostly uniform along the sectional line until reaching the peak load and severely increasing in FPZ during necking.

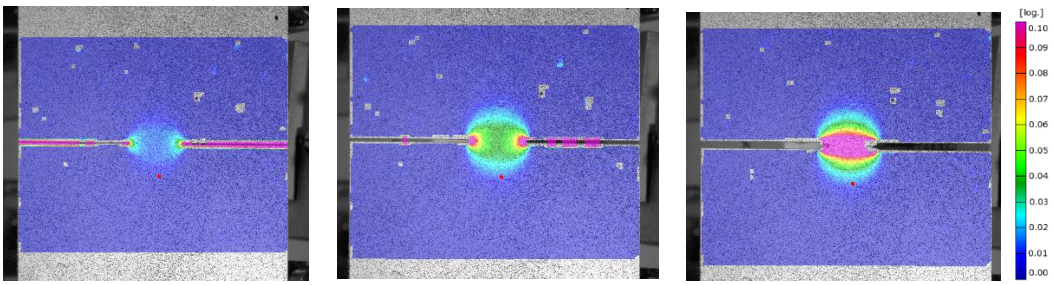

Figure 9. Von-Mises strain around the ligament at different stages during EWF testing for a ligament length of 7.89 mm: (**a**) 50 s; (**b**) 70 s; (**c**) 98 s.

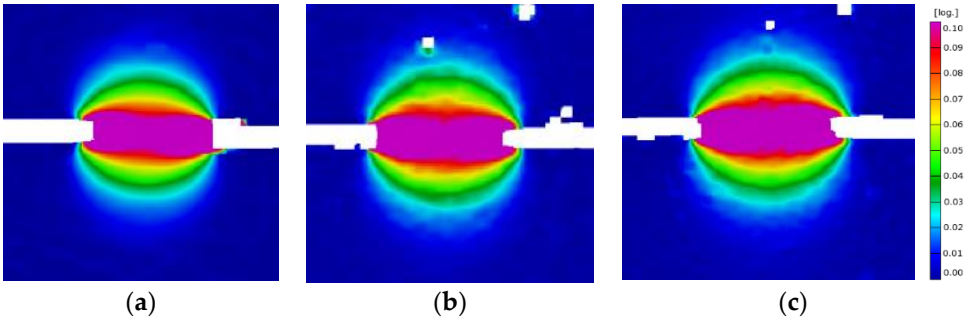

Figure 10. Von-Mises strain around the ligament for various ligament lengths: (**a**) 5.85 mm; (**b**) 8.79 mm; (**c**) 13 mm.

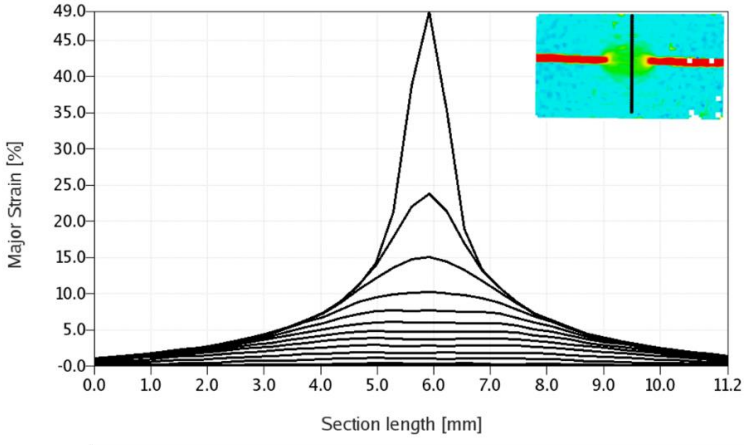

Figure 11. Major strain development along the section line in incremental stage time.

4. Conclusions

Fracture toughness analysis of DP450 steel using essential work of fracture methodology has been completed successfully. Fatigue crack presence strongly influences the w_e and δ_c^e values and has a relatively low impact on ψ^e values. For a quick comparison between two materials, the presence of fatigue crack is not essential, but the results do not truly represent the actual fracture resistance.

Since w_e and δ_c^e values are obtained from extrapolating the curves to zero ligament length, values are not extremely precise in repetition and influenced by the choice of lower ligament lengths. Fractured surfaces have a small flat ductile fracture at the middle and shear lipped slant fracture at the edges. Energy consumed to fracture increases linearly with ligament length; good linearity is observed for notched and fatigue pre-cracked samples. Constant transitional distance is observed in all fractured specimens irrespective of the ligament length. Fracture strain in the FPZ is far higher than the rest of the plastic zone, due to extensive necking before final separation.

Comparing the specific essential work of fracture and *J*-integral at various stages, such as crack initiation and yielding, may give a comprehensive link between two parameters.

Author Contributions: Conceptualization, S.K.M.R. and E.S.; Methodology, S.K.M.R., E.S., F.B. and N.V.L.; Investigation, S.K.M.R., E.S., P.K. and D.M.; Resources, E.S., P.K. and D.M.; Data curation, S.K.M.R., E.S., P.K., D.M. and F.B.; Writing—original draft preparation, S.K.M.R. and E.S.; Writing—review and editing, E.S., N.V.L. and F.B.; Visualization, S.K.M.R., E.S. and N.V.L. All authors have read and agreed to the published version of the manuscript.

Funding: This study has been accomplished by support of the Grant No: SGS_2020_009.

Acknowledgments: We would like to thank Jakub Zajíc, Research Assistant, University of Pardubice, for his support during testing. We would like to thank Skoda Auto, Czech Republic, for providing materials.

Conflicts of Interest: The authors declare no conflict of interest.

Nomenclature

A_g	elongation at ultimate stress
A_{50}	elongation at the fracture
J_c	critical *J*-integral
W_e	essential work of fracture
W_f	total work of fracture
W_p	non-essential work of fracture
u_f	elongation at fracture
w_e	specific essential work of fracture
w_p	specific non-essential work of fracture
w_f	specific work of fracture
L	length of the ligament
n	strain hardening exponent
W	specimen width (DENT)
δ_c^e	crack tip opening displacement from EWF test
ρ_c	critical notch tip radius
σ_u	ultimate tensile strength
σ_y	yield strength
ψ^e	crack tip opening angle from EWF test
t	thickness of the specimen
β	shape factor of plastic deformation

Abbreviations

AHSS	Advanced high strength steels
CTOA	Crack tip opening angle
CTOD	Crack tip opening displacement
DENT	Double edge notch tension
DIC	Digital image correlation
EDM	Electrical discharge machining
EWF	Essential work of fracture
FLD	Forming limit diagram
FPZ	Fracture process zone

References

1. Schmitt, J.H.; Iung, T. New Developments of Advanced High-Strength Steels for Automotive Applications. *Comptes Rendus Phys.* **2018**, *19*, 641–656. [CrossRef]
2. Li, Y.; Song, R.; Jiang, L.; Zhao, Z. Strength Response of 1200 MPa Grade Martensite-Ferrite Dual-Phase Steel under High Strain Rates. *Scr. Mater.* **2019**, *164*, 21–24. [CrossRef]
3. Huang, T.T.; Gou, R.B.; Dan, W.J.; Zhang, W.G. Strain-Hardening Behaviors of Dual Phase Steels with Microstructure Features. *Mater. Sci. Eng. A* **2016**, *672*, 88–97. [CrossRef]
4. Farzam Rad, V.; Khamedi, R.; Moradi, A.R. The Effect of Martensite Volume Fraction on Topography of Dual Phase Steels. *Mater. Lett.* **2019**, *239*, 21–23. [CrossRef]
5. Ingarao, G.; Di Lorenzo, R.; Micari, F. Analysis of Stamping Performances of Dual Phase Steels: A Multi-Objective Approach to Reduce Springback and Thinning Failure. *Mater. Des.* **2009**, *30*, 4421–4433. [CrossRef]
6. Frómeta, D.; Tedesco, M.; Calvo, J.; Lara, A.; Molas, S.; Casellas, D. Assessing Edge Cracking Resistance in AHSS Automotive Parts by the Essential Work of Fracture Methodology. *IOP Conf. Ser. J. Phys. Conf. Ser.* **2017**, *896*, 12102. [CrossRef]
7. ASTM E399. *Standard Test Method for Linear-Elastic Plane-Strain Fracture Toughness of Metallic Materials*; ASTM International: West Conshohocken, PA, USA, 1997.
8. ASTME1820. *Standard Test Method for Measurement of Fracture Toughness*; ASTM International: West Conshohocken, PA, USA, 2020.
9. ASTM E561. *Standard Test Method for KR Curve Determination*; ASTM International: West Conshohocken, PA, USA, 2019.
10. Anderson, T.L. *Fracture Mechanics Fundamentals and Applications*, 4th ed.; CRC Press: Boca Raton, FL, USA, 2017.
11. Broberg, K.B. Critical Review of Some Theories in Fracture Mechanics. *Int. J. Fract. Mech.* **1968**, *4*, 11–19. [CrossRef]
12. Cotterell, B.; Reddel, J.K. The Essential Work of Plane Stress Ductile Fracture. *Int. J. Fract.* **1977**, *13*, 267–277. [CrossRef]
13. Marchal, Y.; Delannay, F. Influence of Test Parameters on the Measurement of the Essential Work of Fracture of Zinc Sheets. *Int. J. Fract.* **1996**, *80*, 295–310. [CrossRef]
14. Chandra, S.K.; Sarkar, R.; Bhowmick, A.D.; De, P.S.; Chakraborti, P.C.; Ray, S.K. Fracture Toughness Evaluation of Interstitial Free Steel Sheet Using Essential Work of Fracture (EWF) Method. *Eng. Fract. Mech.* **2018**, *204*, 29–45. [CrossRef]
15. Clutton, E.Q. ESIS TC4 Experience with the Essential Work of Fracture Method. *Eur. Struct. Integr. Soc.* **2000**, *27*, 187–199. [CrossRef]
16. Clutton, E. Essential Work of Fracture. *Eur. Struct. Integr. Soc.* **2001**, *28*, 177–195. [CrossRef]
17. Golling, S.; Frómeta, D.; Casellas, D.; Jonsén, P. Investigation on the Influence of Loading-Rate on Fracture Toughness of AHSS Grades. *Mater. Sci. Eng. A* **2018**, *726*, 332–341. [CrossRef]
18. Frómeta, D.; Lara, A.; Molas, S.; Casellas, D.; Rehrl, J.; Suppan, C.; Larour, P.; Calvo, J. On the Correlation between Fracture Toughness and Crash Resistance of Advanced High Strength Steels. *Eng. Fract. Mech.* **2019**, *205*, 319–332. [CrossRef]

19. Hossain, M.M.; Kadam, A.A.; Lee, C.F.; Sue, H.J.; Fiscus, D.M. Numerical Modeling of Essential Work of Fracture on Ductile Polymeric Films. *Eng. Fract. Mech.* **2019**, *212*, 210–220. [CrossRef]
20. Na, S.; Spatari, S.; Hsuan, Y.G. Fracture Characterization of Pristine/Post-Consumer HDPE Blends Using the Essential Work of Fracture (EWF) Concept and Extended Finite Element Method (XFEM). *Eng. Fract. Mech.* **2015**, *139*, 1–17. [CrossRef]
21. Abdellah, M.Y. Essential Work of Fracture Assessment for Thin Aluminium Strips Using Finite Element Analysis. *Eng. Fract. Mech.* **2017**, *179*, 190–202. [CrossRef]
22. Wnuk, M.P.; Read, D.T. Essential Work of Fracture (We) versus Energy Dissipation Rate (Jc) in Plane Stress Ductile Fracture. *Int. J. Fract.* **1986**, *31*, 161–171. [CrossRef]
23. Rink, M.; Andena, L.; Marano, C. The Essential Work of Fracture in Relation to J-Integral. *Eng. Fract. Mech.* **2014**, *127*, 46–55. [CrossRef]
24. Hosford, W.F.; Atkins, A.G. On Fracture Toughness in Tearing of Sheet Metal. *J. Mater. Shap. Technol.* **1990**, *8*, 107–110. [CrossRef]
25. Mai, Y.-W.; Cotterell, B. On the Essential Work of Ductile Fracture in Polymers. *Int. J. Fract.* **1986**, *32*, 105–125. [CrossRef]
26. Frómeta, D.; Parareda, S.; Lara, A.; Molas, S.; Casellas, D.; Jonsén, P.; Calvo, J. Identification of Fracture Toughness Parameters to Understand the Fracture Resistance of Advanced High Strength Sheet Steels. *Eng. Fract. Mech.* **2020**, *229*, 106949. [CrossRef]
27. Cotterell, B.; Pardoen, T.; Atkins, A.G. Measuring Toughness and the Cohesive Stress-Displacement Relationship by the Essential Work of Fracture Concept. *Eng. Fract. Mech.* **2005**, *72*, 827–848. [CrossRef]
28. Faccoli, M.; Cornacchia, C.; Gelfi, M.; Panvini, A.; Roberti, R. Notch Ductility of Steels for Automotive Components. *Eng. Fract. Mech.* **2014**, *127*, 181–193. [CrossRef]
29. Kamat, S.V.; Hirth, J.P.; Zok, F.W. Effects of Notch Root Radius on Crack Initiation and Growth Toughnesses of a Cross-Ply Ti-6Al-4V/SiC Composite. *Acta Mater.* **1996**, *44*, 1831–1838. [CrossRef]
30. Hill, R. On Discontinuous Plastic States, with Special Reference to Localized Necking in Thin Sheets. *J. Mech. Phys. Solids* **1952**, *1*, 19–30. [CrossRef]
31. Terao, N.; Baugnet, A. High-Manganese Dual-Phase Steels, Strengthened by Additional Elements (Cr, Ti, V, W). *J. Mater. Sci.* **1990**, *25*, 848–858. [CrossRef]
32. ASTM E8/E8M. *Standard Test Methods for Tension Testing of Metallic Materials*; ASTM International: West Conshohocken, PA, USA, 2016.
33. Geller, S.; Holeczek, K.; Winkler, A.; Tyczynski, T.; Weber, T.; Gude, M.; Modler, N. Multiscale Characterization and Testing of Function-Integrative Fiber-Reinforced Composites. In *Performance Testing of Textiles: Methods, Technology and Applications*; Elsevier Inc.: Amsterdam, The Netherlands, 2016; pp. 155–176. [CrossRef]
34. Knockaert, R.; Doghri, I.; Marchal, Y.; Pardoen, T.; Delannay, F. Experimental and Numerical Investigation of Fracture in Double-Edge Notched Steel Plates. *Int. J. Fract.* **1996**, *81*, 383–399. [CrossRef]
35. Sarkar, R.; Chandra, S.K.; De, P.S.; Chakraborti, P.C.; Ray, S.K. Evaluation of Ductile Tearing Resistance of Dual-Phase DP 780 Grade Automotive Steel Sheet from Essential Work of Fracture (EWF) Tests. *Theor. Appl. Fract. Mech.* **2019**, *103*, 102278. [CrossRef]